Available online at www.sciencedirect.com
ScienceDirect
International Journal of Mass Spectrometry 263 (2007) 276–288
International Journal of Mass Spectrometry
www.elsevier.com/locate/ijms

Kinetics of the reactions of acetone and glyoxal with O_2^+ and NO^+ ions and application to the detection of oxygenated volatile organic compounds in the atmosphere by chemical ionization mass spectrometry

C. Guimbaud [a], V. Catoire [a,*], A. Bergeat [b], E. Michel [a], N. Schoon [c], C. Amelynck [c], D. Labonnette [a], G. Poulet [a]

[a] *Laboratoire de Physique et Chimie de l'Environnement (LPCE), UMR 6115 CNRS, Université d'Orléans, 3A Avenue de la Recherche Scientifique, 45071 Orléans Cedex 2, France*
[b] *Laboratoire de Physico-Chimie Moléculaire (LPCM), UMR 5803 CNRS, Université Bordeaux I, 33405 Talence Cedex, France*
[c] *Belgian Institute for Space Aeronomy (BISA), Ringlaan 3, B-1180 Brussels, Belgium*

Received 30 January 2007; received in revised form 7 March 2007; accepted 7 March 2007
Available online 12 March 2007

Abstract

In situ measurements of oxygenated volatile organic compounds (OVOC) in the upper troposphere–lower stratosphere (UTLS) have gained strong interest because these compounds may be transported during convective events to the UTLS, where they may contribute to the HO_x budget thus influencing the chemistry of ozone. With the aim to quantify OVOC of similar mass (58 u) by chemical ionization mass spectrometry (CIMS), ion–molecule reactions of acetone and glyoxal with O_2^+ and NO^+ have been studied. O_2^+ reacts at the theoretical collision rate with acetone and glyoxal, with room-temperature rate constant values of $(3.1 \pm 0.7) \times 10^{-9}$ and $(1.8 \pm 0.4) \times 10^{-9}$ cm^3 molecule^{-1} s^{-1}, respectively, independent of pressure. The charge transfer product ion (*m*/*z* 58) and a specific fragment product ion are formed for each reaction. NO^+ reacts with acetone and glyoxal with a rate constant lower than the collision rate in N_2 buffer gas at 1.7 hPa, leading to the formation of the association product in both cases as single reaction product. The rate constants increase with pressure at 295 K for both ranges of 1.2–19.2 hPa N_2 and 1.3–2.6 hPa He, indicating a falloff kinetic regime. These results are analysed using conventional statistical calculations. Consistency of the rate constants is obtained for both buffer gases and pressure ranges employed, and high-pressure limits are in agreement with the collision rate constants. Troe analytical expressions of the rate constants are derived for use under any pressure and temperature. From the reaction kinetics and mechanisms obtained in this study and others, a scheme is discussed to quantify separately acetone, glyoxal, and propanal in the UTLS by CIMS, using NO^+, O_2^+, and H_3O^+ as reagent ions, taking into account potential interferences from other important OVOC such as acetaldehyde and from non-methane hydrocarbons such as *n*-propane, butane and 2-methyl propane.

Keywords: Acetone; Glyoxal; Propanal; Upper troposphere; Ion molecule reaction

1. Introduction

Measurements of oxygenated volatile organic compounds (OVOC) in the upper troposphere–lower stratosphere (UTLS) are very sparse and limited to a few species [1–5]. OVOC play a significant role in the chemical and radiative properties of the UTLS since many of them are photolysed in the UTLS, providing additional sources of HO_x and peroxy radicals and thereby influencing the mixing ratio of ozone, an important greenhouse gas in this atmospheric region [6]. It has been estimated [6] that the HO_x source in the UTLS from the reaction of $O(^1D)$ (generated by ozone photolysis) with water vapour becomes insignificant relatively to the HO_x produced through photolysis of acetone, hydroperoxides (ROOH) and aldehydes (RCHO), as soon as water vapour volume mixing ratios are less than 100 ppm. The relative contribution among these OVOC is a mat-

* Corresponding author.
E-mail address: Valery.Catoire@cnrs-orleans.fr (V. Catoire).

1387-3806/$ – see front matter © 2007 Elsevier B.V. All rights reserved.
doi:10.1016/j.ijms.2007.03.006

ter of debate since only few measurements are achieved so far and most of them are not accurate enough. In the tropical UTLS, many OVOC are not produced *in situ* but transported by deep convection. Since convective injection of HO_x precursors and NO_x occurs simultaneously, ozone can be produced efficiently. *In situ* measurements of OVOC in the UTLS with fast integration time analytical techniques are required during convective events.

Chemical ionization mass spectrometry (CIMS) is established to be a sensitive technique for the detection of most OVOC, and proton transfer reaction mass spectrometry (PTRMS) using H_3O^+ as a reagent ion is the main method employed [7]. However, PTRMS is unable to distinguish between isobaric molecules (*i.e.*, species of same molecular mass) leading to an ambiguous detection of atmospheric species. Acetone, which is one of the major OVOC contributing to the upper tropospheric HO_x budget, has been measured throughout the 0–12 km altitude range over the rain forest in Surinam during the LBA-Claire campaign [8–10] using PTRMS. Williams et al. [10] mentioned that propanal and glyoxal could also contribute to the same signal, because these OVOC with a molecular mass of 58 u, all give proton transfer product ions with the same *m*/*z* 59 when reacting with H_3O^+ [11,12]. Acetone, propanal, and glyoxal atmospheric lifetimes are very different: 5 weeks, 9 h [13], and 1 h [14], respectively. Propanal and glyoxal are therefore expected to be much less abundant than acetone in the UTLS, unless recent production from oxidation of VOC or direct injection into the UTLS during fast convective events takes place. In order to discriminate acetone from other atmospheric species of the UTLS, Kiendler and Arnold [15] have equipped an aircraft-borne experiment with an ion trap mass spectrometer providing the opportunity to carry out collision-induced dissociation of mass selected ions to identify unambiguously OVOC in the UTLS. The few experiments performed could not show significant contribution of glyoxal and propanal to the 58 u OVOC burden in the UTLS. Smith and Španěl [16,17] have developed the selected ion flow tube mass spectrometry (SIFT-MS) technique for the real time identification and quantification of many trace compounds with different chemical functionalities in ground level atmospheric air and in human breath, using NO^+, O_2^+, and H_3O^+ as reagent ions. These reagent ions often allow separation of isobaric compounds, such as aldehydes and ketones, and are promising candidates for the separation of glyoxal, acetone, and propanal in the UTLS. However, ion molecule reaction studies of these reagent ions with acetone, and more especially with glyoxal, are not enough documented to derive a scheme for separate quantification of all isobaric species at 58 u in the UTLS.

The relative importance of glyoxal among the other OVOC in the UTLS has to be explored. Glyoxal is formed by oxidation of anthropogenic and biogenic volatile organic compounds (VOC) [18]. Measurements of glyoxal have been performed by differential optical absorption spectroscopy [19] in Mexico City. Volkamer et al. [20] have shown that glyoxal serves as a novel indicator for fast VOC chemistry. Despite of its very short lifetime (1 h) glyoxal has been recently detected by the ozone monitoring instrument (OMI), a nadir viewing spaceborne imaging spectrograph launched on board of the EOS Aura satellite and from the SCanning Imaging Absorption spectroMeter for Atmospheric CHartographY (SCIAMACHY) on board of ESA's satellite ENVISAT [21,22] over large cities and biomass burning regions. These authors argued that glyoxal could be present in the upper troposphere coming either from oxidation of other VOCs or from fast convection. Jost et al. [23] reported first time *in situ* observations of smoke plumes from fires and observed a plume of air highly enriched in carbon monoxide and particles at altitudes up to 16 km in the boreal region, *i.e.*, several kilometres deep into the stratosphere. Biomass smoke injection into the lower stratosphere by large forest fires has been modelled by Luderer et al. [24] showing that the plume reached the UTLS within 30 min, which is shorter than the lifetime of glyoxal in the troposphere. Glyoxal is also directly emitted in the UT from aircraft. Average speciation of VOC emissions for a commercial aircraft shows that glyoxal represents almost 3% of total VOC mass emissions, slightly larger than acetone [25].

This paper reports ion–molecule reaction studies of acetone and glyoxal with O_2^+ and NO^+, demonstrating that these reagent ions can be used in combination with H_3O^+ to detect acetone, propanal and glyoxal in the UTLS independently, taking advantage of the low relative humidity of this part of the atmosphere. Atmospheric trace gas concentrations derived by CIMS are often based on the knowledge of the rate constants and of the product ion branching ratios determined by laboratory studies using flow tube reactors. Experimental kinetics and mechanisms are investigated at LPCE (Orléans, France) with a variable pressure flow tube reactor under laminar and turbulent flow conditions, and at BISA (Brussels, Belgium) with the complementary selective ion flow tube (SIFT) instrument operating at low pressure and allowing accurate determination of the product ion branching ratios. The measured rate constants for the termolecular reactions of acetone and glyoxal with NO^+ show pressure and buffer gas dependence. In order to analyse the falloff curves obtained, *ab initio* and statistical calculations are used to derive analytical expressions of the NO^+ rate constants as a function of pressure and temperature, applicable to any atmospheric conditions. A scheme is proposed to measure separately acetone, glyoxal, and propanal by CIMS in the UTLS using H_3O^+, O_2^+, and NO^+ as reagent ions.

2. Experimental and theoretical methods

2.1. Rate constants of the ion–molecule reactions and product ion branching ratios

The LPCE flow reactor has already been described elsewhere [26,27]. Briefly, the ion–molecule reactions take place in the inner variable pressure flow tube (87 cm long × 2.3 cm i.d.) with a 2–30 STP $dm^3\ min^{-1}$ (standard temperature and pressure: $T = 273.15$ K, $P = 1013.25$ hPa) carrier gas N_2 flow resulting in a pressure range of 1–20 hPa. N_2 carrier gas flow comes from a liquid nitrogen tank (air liquide, purity >99.9995%). NO^+ or O_2^+ reagent ions are generated in a corona discharge

where a mixture of 2–3 STP cm^3 min^{-1} of NO (stated purity >99.0%) or O_2 (stated purity >99.9995%), respectively, and of 1.5 STP dm^3 min^{-1} of argon are flowing. The stated purity of argon is >99.9999% with less than 0.5 ppm of water to minimize production of H_3O^+ ions in the corona discharge. The discharge is produced between a tungsten needle and a grounded stainless steel cylinder. A permanent voltage (typically −800 V) is applied to the needle and a continuous current (typically −0.3 mA) is delivered. At the downstream end of the tube, a fraction of the reactant and product ions are sampled and focused by ion optics through two differentially pumped chambers, one of which containing a quadrupole ion guide (in the radio-frequency mode only). Ions are selected in a third differentially pumped chamber by a quadrupole mass analyzer and detected by a secondary electron multiplier (SEM).

The rate constants k of all ion–molecule reactions investigated are determined by varying the neutral reagent concentration $[X]$, X being acetone or glyoxal, at a fixed reaction distance z, using the pseudo-first order kinetics relationship:

$$\ln\left(\frac{[R^+]_z}{[R^+]_{z,0}}\right) = -k\tau[X] \quad (1)$$

where $[R^+]_z$ and $[R^+]_{z,0}$ are the ion (O_2^+ or NO^+) count rates collected on the SEM in the presence and absence of the neutral reagent X, respectively, and τ defines the reaction time. The reaction time τ (typically 8 ms) is derived from the measured ion velocity, given the reaction distance. The ion velocity is determined by disturbing the ion flow by an electric pulse and synchronously recording the ion arrival time on the SEM detector by a multichannel analyzer. The neutral reagent concentration, $[X]$, in the flow tube is determined from the knowledge of all pressures and flows measured using calibrated MKS capacitance gauges and mass flow meters.

The LPCE instrument allows for variable pressure kinetics to investigate association termolecular reactions in order to derive third-order rate constants. Experiments are performed under low pressure laminar flow conditions (from 1 to 3 hPa) and high-pressure turbulent flow conditions (above 15 hPa). Acetone and glyoxal concentrations were of the order of 10^9–10^{12} molecules cm^{-3}, depending on the rate constant of the ion–molecule reaction involved ($0.18–3.1 \times 10^{-9}$ cm^3 $molecule^{-1}$ s^{-1}), the reaction time of 7–10 ms and the extent of the reaction (5–90%). The branching ratios for the product ions are obtained at low resolution of the mass analyzer to limit mass discrimination. Precision and uncertainties on rate constants and branching ratios are described in later sections. Comparison is made with acetone and glyoxal reactions also studied at low pressures (1.5 hPa) of He with the SIFT instruments of Smith and co-workers [11,28,29] and of BISA [12], respectively. The SIFT method provides selected primary ions but does not allow for high-pressure kinetic studies. In addition, these SIFT instruments lead to very accurate branching ratios values of the product ions formed, since regular measurements with calibration gases are performed to eliminate mass discrimination effects [30,31]. Therefore, the LPCE and BISA apparatus provide complementary data for the investigation of ion–molecule reactions. The first one provides a wider pressure range (1–20 hPa, N_2 buffer) of investigation relative to the second one (1–3 hPa, He buffer) but is less accurate for the quantification of the mixing ratios of the product ions. New experiments are performed with the BISA instrument, where the reaction of NO^+ with acetone is studied in helium buffer gas at 295 K and at pressures ranging from 1.3 to 2.6 hPa. The experimental setup has been described in detail previously [31,32]. NO^+ ions are produced in a microwave discharge in a mixture of air and water vapour and mass-selected in a quadrupole filter before being injected into the flow tube reactor. A few centimeters upstream the reactant gas inlet small amounts of nitrogen are added to the helium buffer gas in order to quench possible vibrationally excited NO^+ ions before they enter the reaction zone. The acetone flow is determined from the pressure drop in a calibrated glass volume containing a dilute mixture of acetone in helium and was varied by means of a heated (315 K) needle valve which separates the glass bottle from the flow tube reactor. Source and product ions are sampled downstream the reaction zone and analyzed in a quadrupole mass spectrometer. The NO^+/acetone rate constant is determined from the decay of the NO^+ count rate versus acetone concentration and from the reaction time (2.5 ms), which is determined experimentally. The precision and the accuracy of the rate constants are at most 15% (2σ level) and 20%, respectively, leading to a global uncertainty of 25% for the rate constants. For product ions with a branching ratio higher than 5%, the precision on the branching ratio is better than 5% (2σ level) and the overall uncertainty is estimated to be 20%. The uncertainty of the branching ratios is mainly determined by the error on the mass discrimination measurements.

2.2. Preparation, introduction and concentration determination of glyoxal and acetone in the flow tube

Glyoxal (CHOCHO) is prepared in a similar way as described by Dobeck et al. [33] by decomposing its trimeric hydrate precursor (Fluka, stated purity >95%) in a glass vacuum line at 490 K in the presence of excess P_2O_5 and under dry N_2 pressure. During this heating, CO impurities are removed at 370 K by flushing away all gases from the vacuum lines *via* the turbo molecular pump. Glyoxal monomer is collected in a 185 K cooled trap, after passing through two traps cooled with ice baths to remove water vapour. Glyoxal is further purified by trap-to-trap distillation in order to remove formaldehyde impurities which could be present. The glyoxal trap is then stored in a cooling bath (Huber, CC 180) at 220 K and under dark conditions for later use. Mixtures of glyoxal (0.1–1 hPa) with N_2 (1050 hPa, air liquide: stated purity >99.9995%) are prepared by sublimation of glyoxal in a 10.37 l bulb. The cooling bath is warmed up to 250 K. The first vapours of glyoxal are always pumped out before filling the bulb up to the desired vapour pressure (MKS capacitance gauge 0–10 Torr; 0.001 Torr full scale range accuracy (FSR)) and adding N_2 slightly above atmospheric pressure (MKS capacitance gauge 0–1000 hPa; 0.1 hPa FSR accuracy). In order to ensure a homogeneous mixing, the mixtures are left to stand for

at least 3 h prior to use for ion–molecule reaction studies or for spectral measurements to check the concentration and purity.

Since formaldehyde (HCHO) is expected to be the main impurity from glyoxal preparation, the mixing ratios of glyoxal and formaldehyde in the bulb are also measured from UV absorption spectroscopy using absorption cross sections of formaldehyde [34] and glyoxal [14] at 285.6, 294.9, 301.25, and 338.75 nm wavelengths. Mixing ratios of glyoxal are equal to $(99.8 \pm 0.6)\%$ (2σ) of the ones directly calculated from preparation and dilution in the mixing bulb. The mixing ratio of formaldehyde is always below 0.1% of the one of glyoxal.

Glyoxal/N_2 mixtures are introduced in the flow tube through a concentric line located at 94.1 cm upstream the sampling cone of the ions. The mixture flow is regulated by a needle valve and the pressure drop is measured as a function of time using a MKS capacitance gauge 0–1000 hPa; 0.1 hPa FSR accuracy). The glyoxal concentration [glyoxal] (molecule cm^{-3}), in the flow tube is derived from Eq. (2) using a convenient unit system:

$$[\text{glyoxal}] = \frac{10^{-4}\, P_{FT} T^{\circ}\, \Delta P_b\, V_b X_b}{k_B T_{FT} T_b P^{\circ}\, \Delta t\, Q^{\circ}_{FT}} \quad (2)$$

where Q°_{FT} is the overall mass flow rate (STP $dm^3\,min^{-1}$) of the gases in the flow tube, P_{FT} the average flow tube pressure in the reaction zone (hPa), ΔP the pressure drop in the bulb (hPa) measured within the period of Δt (min), T_{FT} the average temperature of the gases in the reaction zone (K), T_b the average temperature of glyoxal in the bulb (K), X_b the volumetric mixing ratio of the neutral reagent N in the bulb, V_b the volume of the bulb (10.37 dm^3), P° the standard pressure (1013.25 hPa), T° the standard temperature (273.15 K) and k_B is the Boltzmann constant (1.381×10^{-23} J K^{-1}). The systematic error estimated on the glyoxal concentration is 20% $(2\sigma$ level) including all uncertainties in the parameters given above.

Acetone (CH_3COCH_3) is prepared in two different ways. Liquid acetone is used (Merck, stated purity >99%). In the first method the liquid acetone is vaporized up to 1 hPa (240 K) in a mixing bulb where N_2 is added as described for glyoxal. Acetone concentration is then derived from the same Eq. (2) used for glyoxal. The acetone/N_2 mixture is flowing through the inlet port located at 94.1 cm downstream the flow tube. In a second method (Fig. 1), the liquid acetone is introduced in a small stainless steel reservoir. The acetone is controlled by a liquid mass flow meter (Bronkhorst HI TEC), Q°_1, where the flow rate varies from 0.024 to 0.48 g h^{-1}, *i.e.*, from 1.55×10^{-4} to 3.09×10^{-3} STP $dm^3\,min^{-1}$ in the case of acetone. Acetone is mixed with N_2 gas (air liquide: stated purity >99.9995%) *via* Q°_2 (200–1000 STP $dm^3\,min^{-1}$) and delivered to a controlled temperature evaporator mixer (Bronkhorst HI TEC) where acetone is completely vaporized before introduction *via* Q°_3 (1–10 STP $dm^3\,min^{-1}$) in the movable injector of the flow tube. The flux of acetone varies within a range of 3 decades from 10^{15} to 10^{18} molecules min^{-1} leading to a volumetric mixing ratio of acetone in the flow tube between 10 ppb to 10 ppm.

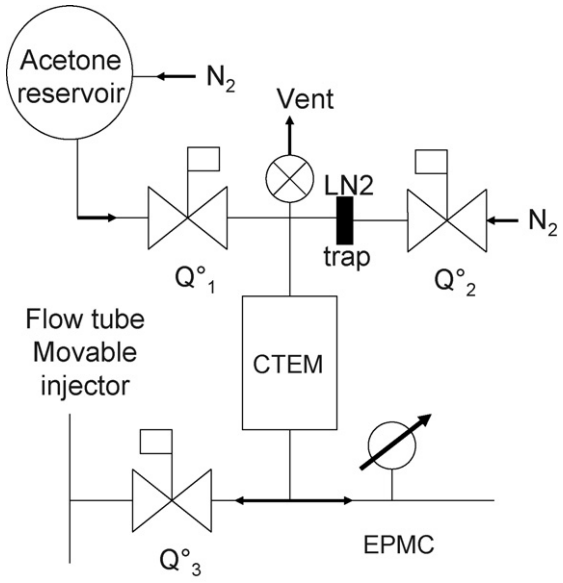

Fig. 1. Setup of acetone injection into the flow tube *via* a movable injector. CTEM: controlled temperature evaporator mixer (Bronkhorst HI TEC); Q°_1: liquid mass flow meter (Bronkhorst HI TEC, 0.48 g h^{-1} or 3.1×10^{-3} STP $dm^3\,min^{-1}$ FSR); Q°_2: MKS mass flow meter (1000 STP $dm^3\,min^{-1}$ FSR); Q°_3: MKS mass flow meter (10 STP $dm^3\,min^{-1}$ FSR); EPMC: electronic pressure meter controller (El press, Bronkhorst HI TEC).

The acetone concentration [acetone], in molecule cm^{-3}, in the flow tube is derived from Eq. (3) using a convenient unit system:

$$[\text{acetone}] = \frac{10^{-4}\, P_{FT} Q^{\circ}_1 Q^{\circ}_3}{k_B T_{FT} Q^{\circ}_2 Q^{\circ}_{FT}} \quad (3)$$

where Q°_1, Q°_2, Q°_3 and Q°_{FT} are given in STP $dm^3\,min^{-1}$. The systematic error estimated on the acetone concentration is 15% (2 σ level) including all uncertainties in the flows involved for the dilution of acetone. In addition, a 15% statistical error (from experimental reproducibility) is measured with this setup and leads to a global uncertainty of 21% $(2\sigma$ level) similar to the first method for the determination of the acetone concentration in the flow tube.

Rate constants from both methods are obtained with a global uncertainty of 25% (2σ) given by the uncertainties in Eq. (1), and adding the uncertainties on both reaction time τ and ion count rates.

2.3. Ab initio and statistical calculations

The reactions of acetone and glyoxal with NO^+ being three body reactions, their rate constants are theoretically pressure-dependent. In the high-pressure limit range, the association rate is the capture rate. But when pressure is lowered, falloff effects come into play and the association rate becomes lower than this capture rate. Calculation of the pressure-dependent association rate constant is performed using conventional statistical calculations in order to reproduce experimental work in N_2 as buffer gas and to verify the consistency with the experimental data in He. The statistical calculations were fitted to these experimen-

Table 1
Molecular parameters for the NO^+ + acetone and NO^+ + glyoxal reactions

Vibrational frequencies (cm^{-1})	
NO^+	2084
Acetone	3045, 3044, 2988, 2981, 2934, 2927, 1753, 1458, 1441, 1437, 1433, 1359, 1357, 1198, 1087, 1053, 863.0, 860.3, 756.2, 511.1, 468.0, 361.3, 130.7, 39.05
$[(CH_3)_2CONO]^+$	3068, 3067, 3008, 2997, 2938, 2931, 2098, 1585, 1444, 1432, 1414, 1403, 1359, 1348, 1236, 1075, 1052, 906.4, 868.0, 783.6, 643.7, 475.0, 421.1, 382.5, 229.8, 132.5, 129.0, 99.69, 86.09, 65.89
trans-Glyoxal	2859, 2853, 1754, 1750, 1337, 1296, 1031, 1027, 785.4, 534.3, 321.1, 140.4
$[(CHO)_2NO]^+$	2947, 2945, 2142, 1760, 1643, 1312, 1278, 1019, 955.8, 813.3, 540.1, 483.9, 317.0, 185.6, 151.9, 114.0, 79.24, 53.92
Rotational constants (cm^{-1})	
NO^+	1.960
Acetone, $\sigma = 2$	0.163, 0.282, 0.336
$[(CH_3)_2CONO]^+$	0.052, 0.063, 0.264
trans-Glyoxal, $\sigma = 2$	0.146, 0.159, 1.859
$[(CHO)_2NO]^+$	0.039, 0.040, 1.027
Enthalpy difference between the reactants and the adduct ($kJ\,mol^{-1}$): ΔH_0°	
NO^+ + acetone	189.2
NO^+ + *trans*-glyoxal	120.8

DFT-B3LYP/6-311 + G(3df,2p) calculations with a correcting factor of 0.9614 for the vibrational frequencies.

tal data and used to perform extrapolations to the atmospheric pressure and temperature.

Statistical calculations are carried out using the "FALLOFF" program [35], modified to introduce the 4–12 Lennard–Jones potential for the centrifugal correction factors [36] and using for the collision number Z_{ID} for the adduct per unit concentration per unit time [37], such as given here by the Langevin rate constant for collisions between the non-polar buffer gas and the ion adduct.

The structural and thermochemical parameters necessary to perform calculations are obtained from quantum chemistry calculations and are given in Table 1. These calculations were carried out using the GAUSSIAN 98 program package [38]. The density functional theory with the Becke's three-parameter hybrid functional of Lee, Yang and Parr, B3LYP [39,40], and the basis sets 6-31G(d) for the geometry optimizations and 6-311 + G(3df,2p) for the energy calculations have been used throughout. The vibrational frequencies have also been obtained in the same way and multiplied by 0.9614 [41].

3. Results and discussion

Room-temperature measured rate constants (k) for reactions obtained in this study are presented in Table 2 and compared to the collision rate constants (k_{SC}) calculated using the parameterized trajectory formulation of Su and Chesnavich [42] and updated by Su [43]. The determination of the latter requires the values of the dipole moment μ_D and the polarizability α of the neutral reactants. Table 3 contains the branching ratios of the product ions for each ion–molecule reaction at the same pressure and temperature (295 K) conditions.

3.1. Reactions of acetone and glyoxal with O_2^+

The room-temperature measured rate constant for the reaction of acetone with O_2^+ is $(3.1 \pm 0.7) \times 10^{-9}\,cm^3\,molecule^{-1}\,s^{-1}$ in the range 1.3–3.4 hPa of N_2 (set of 21 experiments). It is in excellent agreement with the measured ones reported by Španěl et al. [11],

Table 2
Calculated and experimental room-temperature rate constants for the reactions of acetone, glyoxal, and propanal with H_3O^+, NO^+, and O_2^+

Species	α[a]	μ[a]	H_3O^+		NO^+		O_2^+		Pressure (hPa)
			k_{sc}[b]	k[c]	k_{sc}[b]	k[c]	k_{sc}[b]	k[c]	
Acetone	6.4[d], 6.39[e]	2.88[d]	4.1	–	3.5	2.3[f], 1.7[g]	3.4	3.1[f]	1.7N_2[f], 1.5He[g]
Glyoxal	4.74[e]	0.012[e]	1.35	1.9[h]	1.2	0.18[f], 0.075[h]	1.1	1.8[f], 1.5[h]	1.7N_2[f], 1.5He[h]
Propanal	6.5[d], 6.36[e]	2.52[d]	3.6	–	3.1	2.5[i]	3.0	3.1[i]	0.7He[i]

[a] Polarizability α in units of $10^{-24}\,cm^3$ and dipole moments μ in units of Debye.
[b] Calculated collisional rate constants k_{SC} with units of $10^{-9}\,cm^3\,molecule^{-1}\,s^{-1}$ [42,43].
[c] Experimental rate constants with units of $10^{-9}\,cm^3\,molecule^{-1}\,s^{-1}$.
[d] Experimental values [59].
[e] *Ab initio* calculated values (B3LYP/aug-cc-pVDZ) [41].
[f] This work (with N_2 buffer gas).
[g] This work (with He buffer gas).
[h] Michel et al. [12].
[i] Španěl et al. [11].

Table 3
Branching ratios of product ions measured for the reactions of acetone, glyoxal, and propanal with H_3O^+, NO^+, and O_2^+

Species	H_3O^+			NO^+			O_2^+		
	Product ions	amu	B.R. (%)	Product ions	amu	B.R. (%)	Product ions	amu	B.R. (%)
in Acetone, CH_3COCH_3	$C_3H_6O{\cdot}H^+$	59	100[a,b]	$NO^+{\cdot}C_3H_6O$	88	100[a,b]	$C_3H_6O^+$	58	62[a], 60[b]
							$C_2H_3O^+$	43	38[a], 40[b]
Glyoxal[a,c], CHOCHO	$C_2H_2O2{\cdot}H^+$	59	98	$NO^+{\cdot}C_2H_2O_2$	88	100	$C_2H_2O_2^+$	58	49
			2				$HCHO^+$	30	48
							HCO^+	29	3
Propanal[b], C_2H_5CHO	$C_3H_6O{\cdot}H^+$	59	100	$C_3H_5O^+$	57	100	$C_3H_6O^+$	58	50
							$C_3H_5O^+$	57	50

B.R. (%): branching ratio of the product ions in percent.
[a] This work (1.7 hPa N_2).
[b] Španěl et al. [11].
[c] Michel et al. (1.5 hPa He) [12].

$(2.7 \pm 0.5) \times 10^{-9}$ cm^3 molecule^{-1} s^{-1}, and Smith et al. [29], $(3.1 \pm 0.6) \times 10^{-9}$ cm^3 molecule^{-1} s^{-1}, obtained at 300 K in 0.7 hPa of He and relative to the rate constant of acetone with H_3O^+, and with the calculated collision rate constant, $(3.4 \pm 0.7) \times 10^{-9}$ cm^3 molecule^{-1} s^{-1}. The reaction proceeds by non-dissociative and dissociative charge transfer,

$$CH_3COCH_3 + O_2^+ \rightarrow CH_3COCH_3^+ + O_2 \quad (4a)$$

$$CH_3COCH_3 + O_2^+ \rightarrow CH_3CO^+ + CH_3 + O_2 \quad (4b)$$

The non-dissociative charge transfer product ion ($CH_3COCH_3^+$, *m/z* 58) and the fragment product ion (CH_3CO^+, *m/z* 43) are observed in 1.7 hPa in N_2, with branching ratios of $62 \pm 7\%$ and $38 \pm 7\%$, respectively, where quoted uncertainties are global, including experimental scatter (2σ, 7 sets of experiments) and maximum mass discrimination of 15%. This result is similar to the one given by Španěl et al. [11], who found 60% for channel (4a) and (40)% for channel (4b), in 0.7 hPa of He. Moreover, no significant pressure dependence of these branching ratios is observed in our experiments conducted in N_2 between 1.3 and 3.4 hPa, confirming the absence of buffer gas effect, as anticipated by comparing our results with those of Španěl et al. [11]. The occurrence of the non-dissociative charge transfer channel (4a) is consistent with the fact that the ionization energy of acetone, 9.703 eV is smaller than the ionization energy of O_2^+, 12.07 eV [41], giving a reaction exothermicity of 2.367 eV (228 kJ mol^{-1}) which is a good indication that the reaction is exergonic ($\Delta G < 0$) as the entropy change is usually low ($T\Delta S < 10$ kJ mol^{-1} at room temperature) for charge transfer reactions [44]. Dissociative channel (4b) is also exothermic by 1.70 eV (164 kJ mol^{-1}), given the appearance energy of the acetyl cation CH_3CO^+ from acetone (10.37 eV [41]).

The measured reaction rate constant for the reaction of glyoxal with O_2^+ is $(1.8 \pm 0.4) \times 10^{-9}$ cm^3 molecule^{-1} s^{-1} in N_2 buffer gas at 1.7 hPa and is in agreement with the one measured with the BISA SIFT instrument, $(1.5 \pm 0.4) \times 10^{-9}$ cm^3 molecule^{-1} s^{-1}, in He buffer gas at 1.5 hPa [12]. This result gives confidence in the validity of other kinetic data obtained for the same molecule with NO^+ ion in both LPCE and BISA instruments. This rate constant is slightly higher than the calculated one, $(1.1 \pm 0.2) \times 10^{-9}$ cm^3 molecule^{-1} s^{-1}, in the staggered (*trans*) conformation. It is to be noted that this one is derived from *ab initio* calculations (B3LYP/aug-cc-pVDZ) of the polarizability and dipole moment [41], whereas that of acetone is inferred from experimental values of these parameters. The comparison is made with the staggered conformation since it is the most stable form of glyoxal with a fractional population more than 99.9% at 295 K [45]. Since its permanent dipole moment is almost equal to zero, it corresponds to the Langevin capture collision rate constant. Therefore, no pressure dependence for the rate constant is expected, which is indeed observed in the range 1.7–18.6 hPa (with 2.2 and 10.7 hPa as intermediate pressures).

The reaction proceeds by non-dissociative and dissociative charge transfer,

$$CHOCHO + O_2^+ \rightarrow CHOCHO^+ + O_2 \quad (5a)$$

$$CHOCHO + O_2^+ \rightarrow CH_2O^+ + CO + O_2 \quad (5b)$$

$$CHOCHO + O_2^+ \rightarrow CHO^+ + HCO + O_2 \quad (5c)$$

with the product ions, $CHOCHO^+$ (*m/z* 58), CH_2O^+ (*m/z* 30) and CHO^+ (*m/z* 29) observed with branching ratios in agreement with those reported with the BISA instrument, *i.e.*, 49%, 48%, and 3%, respectively at 1.5 hPa in He [12]. The non-dissociative charge transfer mechanism (5a) is consistent with the fact that the ionization energy of glyoxal, 10.200 eV [41], is also lower than the O_2 ionization energy, leading to 1.87 eV (180 kJ mol^{-1}) exothermicity. The dissociative charge transfer channel (5c) is less exothermic, by 0.87 eV (84 kJ mol^{-1}), given the appearance energy of the CHO^+ cation (11.2 eV, [41]). Reaction enthalpy of channel (5b) is calculated to be -122 kJ mol^{-1}, assuming that CH_2O^+ is the ionized form of formaldehyde and using NIST data [41]. So this channel is more exothermic than channel (5c) and leads to a much higher branching ratio. The branching ratios for the non-dissociative charge transfer channel (5a) do not show a significant increase with pressure.

From these studies, it can already be concluded that O_2^+ reacts rapidly with acetone and glyoxal, with rate constants that are pressure independent and in agreement with the ones calcu-

lated with the parameterized equation of Su [43]. In addition to a common mass charge transfer product ion (*m/z* 58), specific fragment product ions CH_3CO^+ (*m/z* 43) and CH_2O^+ (*m/z* 30) with mixing ratios of 38% and 48% are observed for acetone and glyoxal, respectively. Since the charge transfer product ions are not favoured with the increase of pressure, the O_2^+ reagent ion is a potential candidate to distinguish acetone from glyoxal in the atmosphere by CIMS. This possibility is discussed in detail in Section 3.3.

3.2. Reactions of acetone and glyoxal with NO^+

3.2.1. Reaction of acetone with NO^+

The measured rate constant at 295 K in 1.7 hPa N_2 for the reaction of acetone with NO^+, $(2.3 \pm 0.5) \times 10^{-9}$ cm^3 molecule^{-1} s^{-1}, is higher than that measured by other authors at lower pressure in another buffer gas (He), and shows a pressure dependence. Room-temperature rate constants measured from Španěl et al. [11], Fairley et al. [28], and Smith et al. [29] are $(1.2 \pm 0.2) \times 10^{-9}$ cm^3 molecule^{-1} s^{-1}, $(1.3 \pm 0.3) \times 10^{-9}$ cm^3 molecule^{-1} s^{-1}, and $(1.8 \pm 0.2) \times 10^{-9}$ cm^3 molecule^{-1} s^{-1}, under experimental conditions of 0.67, 0.59, and 0.93 hPa He, respectively. All data are significantly lower than the calculated collision rate constant, $(3.5 \pm 0.7) \times 10^{-9}$ cm^3 molecule^{-1} s^{-1}. The rate constant has been also measured as a function of pressure at 295 K in N_2. It increases from $(1.9 \pm 0.4) \times 10^{-9}$ cm^3 molecule^{-1} s^{-1} at 1.2 hPa (2.9×10^{16} molecules cm^{-3}) to $(2.8 \pm 0.7) \times 10^{-9}$ cm^3 molecule^{-1} s^{-1} at 19.2 hPa (4.7×10^{17} molecules cm^{-3}), with intermediate data shown in Fig. 2, in particular $(2.6 \pm 0.7) \times 10^{-9}$ cm^3 molecule^{-1} s^{-1} at 2.8 hPa (6.9×10^{16} molecules cm^{-3}). The measured rate constant at 19.2 hPa in N_2 seems thus to be in the high-pressure range, and in agreement with the calculated collision rate constant. In addition, new experiments have been performed in the range 1.2–2.6 hPa He with the BISA SIFT instrument (Fig. 2), also showing pressure dependence, but with lower rate constant values than in N_2 buffer, *e.g.*, $(1.7 \pm 0.4) \times 10^{-9}$ cm^3 molecule^{-1} s^{-1} at 1.5 hPa He. In contrast, Fairley et al. [28] did not observe significant variation of the rate constant between 0.33 and 0.93 hPa in He. All these results are shown in Fig. 2 and are analysed in detail in the next paragraph, using statistical calculations. The rate constants are in the falloff region and the high-pressure limiting rate constants are not reached at any reported pressure of He but seems to be reached at the higher pressures of N_2. This kinetic behaviour is explained by a three-body association mechanism. The $NO^+ \cdot CH_3COCH_3$ adduct is indeed observed with a branching ratio of 100%, in agreement with all other previously published results quoted above:

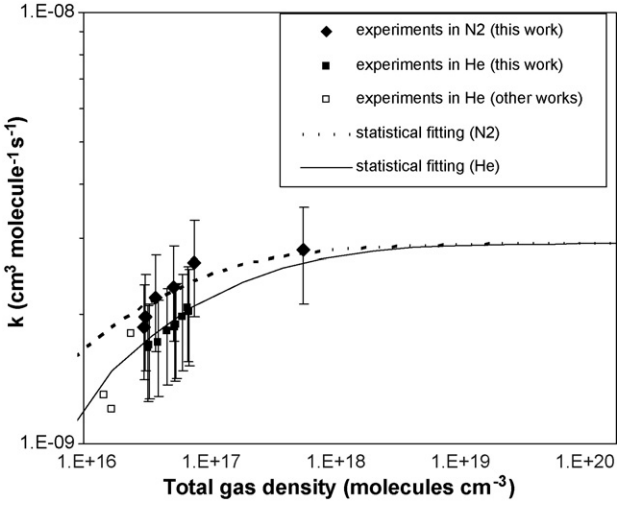

Fig. 2. Pressure dependence of the rate constant of the association reaction (NO^+ + acetone) in N_2 and He buffer gases. The full square and diamond symbols represent the experimental data, and the solid lines are the statistical fitting to the data. Other works in He [11,28,29] are shown (open squares).

$$NO^+ + CH_3COCH_3 \Leftrightarrow NO^+ \cdot CH_3COCH_3^* \quad (6)$$

$$NO^+ \cdot CH_3COCH_3^* + M \rightarrow NO^+ \cdot CH_3COCH_3 + M, \quad (7)$$

Since the ionization energy of acetone, 9.703 eV, is larger than the one of NO, 9.264 eV [41], charge transfer with ground state NO^+ is excluded. Therefore, another exothermic pathway such as association is expected. The association mechanism is the usual pathway for the reactions of ketones with NO^+ [46,47].

Experimental rate constants obtained in different buffer gases (He and N_2) cannot be directly compared for termolecular reactions in their falloff regime for these association mechanism. In order to check the consistency of the different sets of rate constants and their falloff behaviour, experimental results were analysed using *ab initio* and conventional statistical calculations. The experimental rate constant of the NO^+ + acetone reaction versus the total gas density, N_2 being the buffer gas reaches a plateau around 2.8×10^{-9} cm^3 molecule^{-1} s^{-1}. However, the high-pressure limiting association rate constant obtained by the Canonical Flexible Transition State Theory (CFTST) [48] is found to be 4.2×10^{-9} cm^3 molecule^{-1} s^{-1}, which is too high. The model was thus adjusted in order to reproduce the experimental data at the highest pressure of the NO^+ + acetone reaction. Then, the collision efficiency β_c and the exothermicity of the association reaction ΔH_0° were adjusted to reproduce the pressure dependences of the experimental rate constants with N_2 as buffer gas. The β_c value was then fitted to reproduce the experimental data with He as buffer gas, the other parameters being unchanged. Both collision efficiencies values are reasonable, which confirms the agreement between the two sets of experimental data (see Table 4 and Fig. 2). The exothermicity of the NO^+ + acetone reaction would thus be around 178 kJ mol^{-1}, which is close to the B3LYP calculated value (189.2 kJ mol^{-1}). In fact, it seems that the overestimation of the charge transfer exothermicity with the DFT method, as it has already mentioned earlier [49], leads to a too high binding B3LYP calculated energy.

3.2.2. Reaction of glyoxal with NO^+

The room-temperature rate constant value for the reaction NO^+ + glyoxal, $(1.8 \pm 0.4) \times 10^{-10}$ cm^3 molecule^{-1} s^{-1} in N_2 buffer gas at 1.7 hPa, is higher than the one measured of $(7.5 \pm 1.5) \times 10^{-11}$ cm^3 molecule^{-1} s^{-1} in He buffer gas

at 1.5 hPa [12] and is also much lower than the collisional rate constant for the *trans*-glyoxal, derived from the calculations of Su [43], $(1.2 \pm 0.2) \times 10^{-9}$ cm^3 molecule^{-1} s^{-1}. This behaviour is explained by the formation of the NO^+·CHOCHO association product, which was also observed in the previous work of Michel et al. [12] at BISA. This results from a mechanism similar to Eqs. (6) and (7) for which the second order high-pressure limiting rate constant is not reached at 1.7 hPa. The ionization energy of glyoxal, 10.2 eV [41], is larger than that of NO (9.264 eV), excluding again charge transfer with ground state NO^+. Charge transfer is generally endothermic for saturated aldehydes and these ones usually react with NO^+ by hydride ion transfer [11,47,50]. This is not the present case for the dialdehyde glyoxal, which only forms the association product ion, in contrast with the saturated dialdehyde glutyraldehyde ($CHOCH_2CH_2CH_2CHO$). The rate constant is observed to increase with pressure, reaching $(4.2 \pm 1.0) \times 10^{-10}$ cm^3 molecule^{-1} s^{-1} in N_2 buffer gas at 18.4 hPa (4.5×10^{17} molecules cm^{-3}), as shown in Fig. 3.

The consistency between the rate constant determined previously only in He and the pressure-dependent rate constants measured in N_2 in the present work is checked again by *ab initio* and statistical calculations. The lack of experimental data in the high-pressure range cannot allow any serious adjustment of the calculated limiting high-pressure association rate constant. However, it was decided to test the assumption that this high-pressure rate constant is the collisional one from the Su and Chesnavich approach [42,43], since this has been found experimentally for the acetone + NO^+ reaction. The two parameters, the collision efficiency β_c and the exothermicity ΔH_0° of the association reaction, were then fitted to reproduce the experimental data with N_2 as buffer gas (see Table 4 and Fig. 3). The observation of the same collision efficiencies as for the NO^+ + acetone reaction with the two buffer gases confirms the consistency between the sets of data. The fit leads to the empirical value of 132 kJ mol^{-1} for the NO^+ + *trans*-glyoxal reaction enthalpy. This value is larger than the calculated one (120.8 kJ mol^{-1}; Table 1) but in correct agreement, given the uncertainties on the theoretical method found for the NO^+ + acetone reaction. The success in the fits of both experimental data sets with reasonable β_c and ΔH_0° give thus confidence in the choice of the limiting high-pressure association rate constant value of 1.2×10^{-9} cm^3 molecule^{-1} s^{-1}, in agreement with the collisional rate constant from Su and Chesnavich theory [42,43].

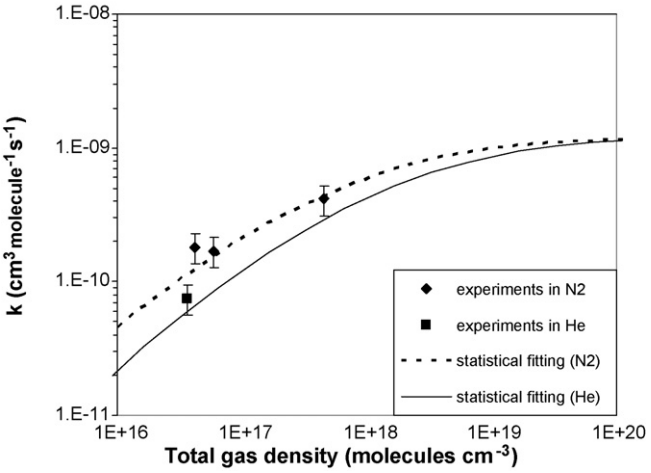

Fig. 3. Pressure dependence of the rate constant for the reaction (NO^+ + glyoxal) in N_2 and He buffer gases. The square and diamond symbols represent the experimental data and the lines are the statistical fitting to the data.

3.2.3. NO^+ reactions and statistical calculations

To summarize, NO^+ reacts with acetone and glyoxal *via* the association process, leading to ion products of similar *m/z* 88, with rate constants that rapidly increase with pressure in the range (0.6–19.2 hPa). This could allow the detection of the total amount of acetone and glyoxal in the UTLS using this reagent ion. One prerequisite is however that the rate constants must be firmly established whatever the buffer gas and pressure. The combination of the experimental data under significant ranges of pressure of two different third bodies (N_2 and He) with the statistical calculation results provides a complete and coherent picture of the kinetics for these ion–molecule association reactions. For both reactions, collision efficiencies are equal, with that of N_2 a factor of two higher than that of He. As CIMS reactors may operate under various pressures of air, the statistical calculations have been performed to extrapolate the experimental kinetic results to atmospheric pressure and temperature ranges. As the limiting high-pressure rate constant for the NO^+ + acetone + N_2 reaction is found to be equal to the collisional value of Su and Chesnavich at room temperature, its temperature dependence may be predicted by this theory [42,43]:

$$k_{\infty\,SC}(T) = 4.26 \times 10^{-8}\, T^{-0.44} \quad (8)$$

For the NO^+ + glyoxal reaction, no temperature dependence was used, as predicted by this theory. The collision efficiency β_c is deduced from the value at 295 K for N_2 buffer gas and its

Table 4
Statistical calculations results at 295 K for the (NO^+ + acetone) and the (NO^+ + glyoxal) reactions

Ion molecule reaction	NO^+ + acetone	NO^+ + glyoxal
ΔH_0° (kJ/mol) used for calculations	178.4	131.6
Equilibrium constant, K_{eq} (cm^3 molecule^{-1})	6.05×10^5	4.86×10^{-3}
High-pressure limiting association rate constant, k_{ass}^∞ (cm^3 molecule^{-1} s^{-1})	2.9×10^{-9}	1.2×10^{-9}
Collision number, Z_{ID} (cm^3 molecule^{-1} s^{-1})	6.72×10^{-10} (N_2 buffer) 5.42×10^{-10} (He buffer)	
Collision efficiency, β_c	0.2 (N_2 buffer) 0.1 (He buffer)	0.2 (N_2 buffer) 0.1 (He buffer)

usual temperature dependence for the exponential transition-probability model is:

$$\frac{\sqrt{\beta_c}}{1-\sqrt{\beta_c}} = \frac{\langle \Delta E \rangle_{down}}{F_E k_B T} \quad (9)$$

where F_E is the correction factor of the energy dependence of the density of states in the adduct XNO^+ and $\langle \Delta E \rangle_{down}$ is the average loss of energy per collision [37,51].

Pressure and temperature dependencies of the rate constants can be presented using the conventional Troe's equation [51,52]:

$$k(T) = \frac{k_0(T)[M]}{1 + (k_0(T)[M]/k_\infty(T))} F_c(T)^{1/(1+(\log(k_0(T)[M]/k_\infty(T)))^2)} \quad (10)$$

in order to provide a quick and convenient way of calculating rate constant values in the range (1.3–10^3) hPa and (200–350) K. The three parameters k_0, k_∞, and F_c have been derived from the non-linear fitting of the above equation to the presented statistical calculated results at various temperatures (eight temperatures). The resulting values of $k_0(T)$, $k_\infty(T)$, and $F_c(T)$ yield the following expressions:

For the NO^+ + acetone reaction:

$$k_0(T) = (3.8 \pm 0.3) \times 10^{-24} \left(\frac{T}{300\,K}\right)^{-(5.6\pm0.2)} cm^6\ molecule^{-2}\ s^{-1} \quad (11a)$$

$$k_\infty(T) = (3.0 \pm 0.3) \times 10^{-9} \left(\frac{T}{300\,K}\right)^{-(0.41\pm0.01)} cm^3\ molecule^{-1}\ s^{-1} \quad (12a)$$

$$F_c(T) = \exp\left(-\frac{T}{(378 \pm 10)\,K}\right) \quad (13a)$$

For the NO^+ + glyoxal reaction:

$$k_0(T) = (8.1 \pm 0.3) \times 10^{-26} \left(\frac{T}{300\,K}\right)^{-(4.60\pm0.1)} cm^6\ molecule^{-2}\ s^{-1} \quad (11b)$$

$$k_\infty(T) = (1.27 \pm 0.03) \times 10^{-9} \left(\frac{T}{300\,K}\right)^{-(0.02\pm0.02)} cm^3\ molecule^{-1}\ s^{-1} \quad (12b)$$

$$F_c(T) = (0.53 \pm 0.01)\ \exp\left(\frac{-T}{(843 \pm 48)\,K}\right) \quad (13b)$$

The expression of Troe with the above parameters yields fairly good representations of the calculated curves for the two reactions, and therefore, of the experimental data. The simple expression for F_c commonly used, $F_c = \exp(-T/C)$, where C is a constant, was not used in the present case, as it did not yield a good representation of the data over the whole temperature range for the NO^+ + glyoxal reaction. The proposed two-parameters expression given above is a simplification of the two-exponential/four-parameter expression proposed by Wagner and Wardlaw [53]; the latter is intended for much wider temperature range than the present one.

However, all these results are highly dependent on the fitted parameters, β_c, ΔH_0° and the limiting high-pressure association rate constants, and experimental results at different temperatures and higher pressures would allow decreasing the uncertainties on these rate constant values. This is specially the case for the NO^+ + glyoxal reaction where the limiting high-pressure rate constant was fixed to the Su and Chesnavich collisional rate constant, given the consistency of the results for acetone and glyoxal in both buffer gases and the fact it was found experimentally for the acetone reaction.

3.3. Selective identification and quantification of acetone, glyoxal, and propanal in the upper atmosphere by CIMS using NO^+, H_3O^+, and O_2^+ as reagent ions

The selected ion flow tube mass spectrometry (SIFT-MS) technique has been developed by Smith and Španěl [16,17], using NO^+, O_2^+, and H_3O^+ as reagent ions, which allows on-line identification and quantification of many isobaric atmospheric trace gases, especially isobaric aldehydes and ketones. In some cases, using NO^+ or O_2^+ reagent ions instead of H_3O^+ ions can result in a more selective detection of some specific organic molecules in ambient air. H_3O^+ undergoes usually proton transfer ion–molecule reactions, leading to ambiguous detection of isobaric species. NO^+ and O_2^+ ion chemistries of isobaric species with different chemical functionalities can be quite different and therefore chemical ionisation by NO^+ and O_2^+ can sometimes be more selective than proton transfer chemical ionisation. Moreover, H_3O^+ undergoes faster ion–molecule reactions with H_2O [54] than NO^+ and O_2^+. The resulting $H_3O^+(H_2O)_n$ reagent ions complicate the product ion spectra and make its interpretation and the quantitative analysis of the trace gases more challenging in ambient air. In the relatively dry UTLS region of the atmosphere, where the water vapour mixing ratio is typically 100 ppm [55], formation of $H_3O^+(H_2O)_n$ ions is still significant and can be a nuisance even in low pressure (about 1 mbar) CIMS flow tube reactors with atmospheric air as buffer gas, whereas formation of $NO^+(H_2O)_n$ and $O_2^+(H_2O)_n$ ions is sufficiently suppressed [54], resulting in less complicated NO^+ and O_2^+ CIMS spectra. NO^+ and O_2^+ reagent ions give specific fragment product ions by reaction with isobaric OVOC allowing then for their specific identification. In less dry atmospheric regions, such as in the troposphere, $NO^+(H_2O)_n$ and $O_2^+(H_2O)_n$ will become more important and initiate in most cases ligand-switching reactions leading then to an impossible detection of isobaric OVOC.

Table 5
Volatile organic compounds with potential interferences in their CIMS spectra: concentrations in the UTLS, rate constants and product ions for their reactions with H_3O^+, NO^+, and O_2^+

Species	H_3O^+			NO^+			O_2^+		
LS (ppt)	Rate constant			Rate constant			Rate constant		
UT (ppt)	Product ions	m/z	B.R.	Product ions	B.R.	%	Product ions	m/z	B.R.
n-Butane [1,2,8]	n.r [1] 0.003 [2]			n.r [1] 0.002 [2]			1.4 [2]		
$CH_3(CH_2)_2CH_3$	0.0016 [8]			0.0025 [8]			$C_4H_{10}^+$	58	20 [1] 25 [2]
0-50 [6]	$C_4H_{10}.H_3O^+$	77	70 [2] 100 [8]	$C_4H_9^+$ [2,8]	57	100	$C_4H_9^+$	57	5 [1]
10-150 [6]	$C_4H_9^+$	57	30 [2] 0 [8]				$C_3H_7^+$	43	65 [1,2]
							$C_3H_6^+$	42	10 [1] 5 [2]
							$C_2H_4^+$	28	5 [2]
2-Methyl propane [1,2,8]	n.r [1] 0.0042 [2]			0.9 [1] 1.0 [2] 0.9 [8]			1.5 [2]		
$CH(CH_3)_3$	0.0018 [8]						$C_3H_7^+$	43	40 [1] 45 [2]
0-7 [6]	$C_4H_{10}.H_3O^+$	77	55 [2] 0 [8]	$C_4H_9^+$ [1,2,8]	57	100	$C_4H_9^+$	57	25 [1]
10-70 [6]	$C_4H_9^+$	57	45 [2] 100 [8]				$C_3H_6^+$	42	25 [1] 55 [2]
							$C_4H_8^+$	56	10 [2]
Ethane [2,8]	< 0.001 [2]			< 0.001 [2]			1.1 [2]		
CH_3CH_3	< 0.0001 [8]						$C_2H_6^+$	30	30
40-500 [6]	unknown [2,8]	unknown	unknown	n.r.			$C_2H_5^+$	29	55
400-1500 [5,6]							$C_2H_4^+$	28	15
Formaldehyde [3]				<0.1			2.2		
HCHO							$HCHO^+$	30	60
-	$HCHO.H^+$	31	100	-	-	-	HCO^+	29	40
<50-80 [5]									
Propane [2,8]	< 0.001 [2]			~ 0.001			1.4 [2]		
$CH_3CH_2CH_3$	0.0003 [8]						$C_3H_8^+$	44	30
0-50 [6]	$C_3H_8.H_3O^+$ [8]	63	100	$C_3H_7^+$	43	100	$C_3H_7^+$	43	35
50-500 [6]							$C_2H_5^+$	29	5
							$C_2H_4^+$	28	25
n-pentane [4,8]				< 0.05 [4]			0.8 [4]		
$CH_3(CH_2)_3CH_3$				0.0039 [8]			$C_3H_7^+$	43	55
				$C_5H_{11}^+$	71	100 [4] 91 [8]	$C_3H_6^+$	42	45
Acetaldehyde [3]	3.7			0.6			2.3		
CH_3CHO							CH_3CHO^+	44	55
220-650 ppt [7]	$CH_3CHO.H^+$	45	100	CH_3CO^+	43	100	CH_3CO^+	43	45

(1) Španěl and Smith [60] in 0.7 hPa in He; (2) Wilson et al. [61] in 0.6 hPa in He; (3) Španěl et al. [11] in 0.7 hPa in He; (4) Španěl and Smith [62] in 0.7 hPa in He; (5) Jaeglé et al. [56]; (6) Scheeren et al. [2]; (7) Singh et al. [4]; (8) Arnold et al. [63].
n.r.: no reaction, B.R.: branching ratio of the product ions in percent.
Units for rate constants are given in 10^{-9} cm^3 s^{-1} $molecule^{-1}$.

Tables 2, 3 and 5 contain all the required information to define pathways for selective identification and quantification of acetone, glyoxal, and propanal in the UTLS by CIMS using NO^+, H_3O^+, and O_2^+ as reagent ions. Kinetics and branching ratios of product ions from acetone, glyoxal, and propanal are given in Tables 2 and 3. Table 5 provides information relative to other VOC that represent potential interferences for the CIMS spectra of acetone, glyoxal, and propanal. Measured concentrations of these VOC in the UTLS and the rate constants of their reactions with H_3O^+, NO^+, and O_2^+, as well as the product ions branching ratios are provided. Ratios of the peak intensities of the product ions to the reagent ions, NO^+, H_3O^+ or O_2^+, can be derived under atmospheric conditions and the concentration expressions of some atmospheric species of interest can be inferred.

For atmospheric trace gas measurements, low conversion rate (≈1%) of the reagent ions is usually used. As a result, the determination of the atmospheric trace gas concentration is independent from the reactions of the reagent ion with other atmospheric species. The low conversion rate is also needed to avoid secondary ion–molecule reactions. The ratio of the product ion intensity $I_{\text{product ion (molecule)}}$ to the reactant ion intensity, I_{ion}, is then given by:

$$\frac{I_{\text{product ion}}}{I_{\text{ion}}} = \sum_i k_i(\text{ion} + \text{molecule}_i)\,[\text{molecule}_i]\,t \qquad (14)$$

where k_i is the rate constant of the ion–molecule$_i$ reaction involved ($cm^3\ s^{-1}$ molecule^{-1}), [molecule$_i$] the concentration of the reactive atmospheric species i (molecules cm^{-3}), and t is the reaction time (s). This approximation is similar to the one described by Lindinger et al. [7] for the detection of OVOC by PTRMS and leads to Eqs. (15) to (19) below.

NO^+ reacts with acetone and glyoxal to give an association product ion (m/z 88) and with propanal to give a hydride transfer product ion (m/z 57). NO^+ undergoes rapid reactions with these species, close to collision rate, except with glyoxal at the lower pressure range usable for a CIMS flow tube reactor (around 1 hPa). According to the previous measurements performed in the UTLS, acetone concentrations vary from 40 to 800 ppt in the LS [2] and from 300 to 2500 ppt in the UT [2,56]. Propanal and glyoxal have never been measured up to now in the UTLS. Other alkanes such as n-butane or 2-methyl propane could contribute to the same signal at m/z 57 from hydride transfer to NO^+. However, since the rate constant of the reaction of NO^+ with n-butane is too low and the concentration of 2-methyl propane is likely too low to contribute significantly to the m/z 57 signal under UTLS conditions, interferences from their product ions can be neglected.

Therefore, NO^+ reacts selectively with acetone and glyoxal to form the product ion at m/z 88 and with propanal to form the product ion at m/z 57. The ratios of the peak intensity at m/z 88 (I_{88}) and at m/z 57 (I_{57}) to the peak intensity at m/z 30 (I_{NO^+}), respectively, are given in Eqs. (15) and (16):

$$\frac{I_{88}}{I_{NO^+}} = [\text{acetone}]\, k_{(NO^+ + \text{acetone})}\, t + [\text{glyoxal}]\, k_{(NO^+ + \text{glyoxal})}\, t \quad (15)$$

where the rate constants k are pressure and temperature dependent and given by the Troe's Eq. (10)

$$\frac{I_{57}}{I_{NO^+}} = [\text{propanal}]\, k_{(NO^+ + \text{propanal})}\, t \quad (16)$$

In addition, the use of H_3O^+ as reagent ion in Eq. (17) would allow for the quantification of acetone, glyoxal, and propanal concentrations:

$$\frac{I_{59}}{I_{H_3O^+}} = [\text{acetone}]\, k_{(H_3O^+ + \text{acetone})} t + [\text{glyoxal}]\, k_{(H_3O^+ + \text{glyoxal})}\, 0.98\, t + [\text{propanal}]\, k_{(H_3O^+ + \text{propanal})} t \quad (17)$$

where I_{59} is the peak intensity at m/z 59 and $I_{H_3O^+}$ is the peak intensity at m/z 19.

The separate quantification of these three species is made by solving Eqs. (15)–(17) in case of equal or significant concentration of glyoxal relative to acetone and at high pressures (rate constant glyoxal/NO^+ near high-pressure limit). Such atmospheric conditions could occur in the UTLS during periods of fast convective events with biomass burning. CIMS for the detection of OVOC could be a good tool to point out this kind of events. At low pressures (small NO^+/glyoxal reaction rate constant) or in the cases where the concentration of glyoxal is not large or much smaller with respect to the one of acetone, Eq. (15) gives acetone concentration, Eq. (16) propanal concentration and then Eq. (17) an estimate of glyoxal concentration.

Concerning the O_2^+ reagent, this one reacts with glyoxal to give two specific fragment product ions (*i.e.*, different from propanal or acetone product ions), $HCHO^+$ (m/z 30) and HCO^+ (m/z 29) with a mixing ratio of 48% and 3%, respectively. However, in ambient UTLS air, the observation of these two signals at m/z 30 and 29 would be attributed mainly to the reaction of ethane with O_2^+, and in a minor part to the reaction of formaldehyde with O_2^+, implying that glyoxal can not be detected by O_2^+ in a direct way since its other product ion (the charge transfer product at m/z 58) has a similar mass as acetone and propanal charge transfer products (see Table 3). O_2^+ also reacts with propanal and acetone to give one specific fragment product ion, $C_2H_5CO^+$ (m/z 57) and CH_3CO^+ (m/z 43), with a mixing ratio of 50%, and 38%, respectively. Using O_2^+ for the detection of propanal is less accurate than the use of NO^+ since the fragment product ion at m/z 57 can be also produced by the reaction of O_2^+ with n-butane, 2-methyl propane and many ketones of higher molecular masses such as butanone and pentanone [11]. However, the main interest for O_2^+ resides in using it as reagent ion for the detection of acetone, in addition to the above method employing only NO^+ and H_3O^+, which gives consistency in deriving glyoxal from the Eqs. (15)–(17). O_2^+ reacts rapidly with acetone, with a rate constant of 3.1×10^{-9} cm^3 molecule^{-1} s^{-1}, to produce a fragment product ion at m/z 43 with a branching ratio of 38%, leading to possible detection of acetone. Indeed, even if other atmospheric species may contribute to the formation of the fragment product ion at m/z 43 these ones can be accurately measured as well, and acetone concentration can therefore be inferred. These other species are mainly acetaldehyde and some non-methane hydrocarbons (NMHC) such as propane, n-butane, 2-methyl propane, n-pentane which produce the same fragment product ion at m/z 43 with significant branching ratio and rate constants higher than 10^{-9} cm^3 molecule^{-1} s^{-1} (see Table 5). Acetaldehyde concentration can be directly measured by proton transfer reaction with H_3O^+ (Eq. (18)) since no proton transfer reaction occurs with propane which has the same molecular mass (44 u). PTRMS is a reliable technique for acetaldehyde measurements [57]. By opposition to OVOC, *in situ* sampling of NMHC from canisters with off-line analysis (such as GC-FID) is reliable since NMHC can be stored for a long period without adsorption or reaction with surfaces. As a consequence, acetone concentration can be derived from Eq. (19) since acetaldehyde and NMHC concentrations can be measured independently:

$$\frac{I_{45}}{I_{H_3O^+}} = [\text{acetaldehyde}]\, k_{(H_3O^+ + \text{acetaldehyde})}\, t \quad (18)$$

$$\frac{I_{43}}{I_{O_2^+}} = [\text{acetone}]\, k_{(O_2^+ + \text{acetone})}\, 0.38\, t + [\text{acetaldehyde}]\, k_{(O_2^+ + \text{acetaldehyde})}\, 0.45\, t + \sum [\text{NMHC}_i]\, k_i\, \text{B.R.}_i\, t \quad (19)$$

I_{45} is the peak intensity at m/z 45 and $I_{H_3O^+}$ is the peak intensity at m/z 19 using H_3O^+ as reagent ion. I_{43} is the peak intensity at m/z 43 and $I_{O_2{}^+}$ is the peak intensity at m/z 32, using $O_2{}^+$ as reagent ion. The rate constants k are given in Table 5. The last term of Eq. (19) is the contribution of each $NMHC_i$ to the formation of the product ion at m/z 43. Branching ratios $B.R._i$ of the product ions for each reaction of $O_2{}^+$ with $NMHC_i$ contributing significantly to the formation of product ion signal at m/z 43 are reported in Table 5. It is assumed that the branching ratio of the product ions of the reaction of acetaldehyde and $NMHC_i$ with $O_2{}^+$ are pressure independent.

To summarize, acetone, glyoxal, and propanal can be obtained from Eqs. (15)–(17) using NO^+ and H_3O^+ as reagent ions. In addition, acetaldehyde concentration can be extracted from Eq. (18), and acetone concentration can also be derived from Eq. (19) using $O_2{}^+$, which gives consistency in deriving glyoxal from Eq. (15) or from Eqs. (16) and (17).

Finally a possible CIMS setup for the *in situ* detection of acetone, glyoxal, and propanal is briefly discussed. One or more selective ion sources capable of alternately producing sufficient amounts of H_3O^+, NO^+, and $O_2{}^+$ reagent ions are needed. Possible ion source candidates could be the discharge ion sources previously used in balloon-borne CIMS experiments [58] and in this work, or a hollow cathode ion source for the production of H_3O^+ ions [7]. Even when using a low pressure ion molecule reactor (≈1 hPa) hydration of H_3O^+ reagent ions may still be significant at the typical water vapour mixing ratio (100 ppm) present in the UTLS, but is less important for NO^+ and $O_2{}^+$ [54].

A mean to keep hydration to a minimum is the use of a drift tube reactor with and without application of an electric field: (i) with an electric field at lower pressure when operating with H_3O^+ to avoid hydration of reagent and product ions, as it is the case in the Lindinger's PTRMS apparatus and (ii) without an electric field at any pressure when operating with NO^+ and $O_2{}^+$, since water clustering of these reagent ions is less significant. For the NO^+ reactions, hydration of the product ions of interest does not occur. Weak or non-existing hydration of the association products resulting from the reaction of NO^+ with ketones and of the hydride ion transfer product ions resulting from the reaction of NO^+ with saturated aldehydes are reported in the literature [46,50].

4. Conclusion

Ion–molecule reactions of acetone and glyoxal with $O_2{}^+$ and NO^+ have been studied with the aim to separately quantify OVOC of similar mass (58 u) by CIMS in the atmosphere. Experimental rate constants have been measured as a function of pressure and analysed using statistical calculations, where Troe's analytical expressions of the rate constants have been derived for use under any pressure and temperature. Product ions branching ratios have been also measured as a function of pressure. From all the data obtained, ionization schemes have been defined to identify unambiguously acetone, propanal and glyoxal in relatively dry atmospheric conditions such as in the UTLS region, which is of great interest as these compounds play an important role in the chemistry and the radiative properties of this part of the atmosphere. NO^+, H_3O^+, and $O_2{}^+$ can be used as reagent ions to measure acetone, propanal and glyoxal, separately.

Acknowledgments

The French "Conseil Régional du Centre" and the French "Programme National de Chimie Atmosphérique (PNCA)" are acknowledged for their financial support.

References

[1] H.B. Singh, Y. Chen, A. Tabazadeh, Y. Fukui, I. Bey, R. Yantosca, D. Jacob, F. Arnold, K. Wohlfrom, D. Atlas, F. Flocke, D. Blake, N. Blake, B. Heikes, J. Snow, R. Talbot, G. Gregory, G. Sachse, S. Vay, Y. Kondo, J. Geophys. Res. A 105 (2000) 3795.
[2] H.A. Scheeren, H. Fischer, J. Lelieveld, P. Hoor, J. Rudolph, F. Arnold, B. Bregman, C. Brühl, A. Engel, C. Van Der Veen, D. Brunner, J. Geophys. Res. A 108. (2003) 4805, doi:10.1029/2003JD003650.
[3] C. Mari, C. Saüt, D.J. Jacob, A. Staudt, M.A. Avery, W.H. Brune, I. Faloona, B.G. Heikes, G.W. Sachse, S.T. Sandholm, H.B. Singh, D. Tan, J. Geophys. Res. A 108 (2003) 8232, doi:10.1029/2001JD001466.
[4] H.B. Singh, L.J. Salas, R.B. Chatfield, E. Czech, A. Fried, J. Walega, M.J. Evans, B.D. Field, D.J. Jacob, D. Blake, B. Heikes, R. Talbot, G. Sachse, J.H. Crawford, M.A. Avery, S. Sandholm, H. Fuelberg, J. Geophys. Res. A 109. (2004) D15S07, doi:10.1029/2003JD003883.
[5] A. Colomb, J. Williams, J. Crowley, V. Gros, R. Hofmann, G. Salisbury, T. Kluepfel, R. Kormann, A. Stickler, C. Forster, J. Lelieveld, Environ. Chem. 3 (2006) 244.
[6] L. Jaeglé, D.J. Jacob, W.H. Brune, P.O. Wennberg, Atmos. Environ. 35 (2001) 469.
[7] W. Lindinger, A. Hansel, A. Jordan, Int. J. Mass Spectrom. 173 (1998) 191.
[8] P.J. Crutzen, J. Williams, U. Pöschl, P. Hoor, H. Fischer, C. Warneke, R. Holzinger, A. Hansel, W. Lindinger, B. Scheeren, J. Lelieveld, Atmos. Environ. 34 (2000) 1161.
[9] U. Pöschl, J. Williams, P. Hoor, H. Fischer, P.J. Crutzen, C. Warneke, R. Holzinger, A. Hansel, A. Jordan, W. Lindinger, H.A. Scheeren, W. Peters, J. Lelieveld, J. Atmos. Chem. 38 (2001) 115.
[10] J. Williams, U. Pöschl, P.J. Crutzen, A. Hansel, R. Holzinger, C. Warneke, W. Lindinger, J. Lelieveld, J. Atmos. Chem. 38 (2001) 133.
[11] P. Španěl, Y. Ji, D. Smith, Int. J. Mass Spectrom. Ion Process. 165/166 (1997) 25.
[12] E. Michel, N. Schoon, C. Amelynck, C. Guimbaud, V. Catoire, E. Arijs, Int. J. Mass Spectrom. 244 (2005) 50.
[13] J. De Gouw, C. Warneke, T. Karl, G. Eerdekens, C. Van Der Veen, R. Fall, Int. J. Mass Spectrom. 223/224 (2003) 365.
[14] A. Horowitz, R. Meller, G.K. Moortgat, J. Photochem. Photobiol. A: Chem. 146 (2001) 19.
[15] A. Kiendler, F. Arnold, Int. J. Mass Spectrom. 223–224 (2003) 733.
[16] D. Smith, P. Španěl, Int. Rev. Phys. Chem. 15 (1996) 231.
[17] D. Smith, P. Španel, Mass Spectrom. Rev. 24 (2005) 661.
[18] R. Volkamer, U. Platt, K. Wirtz, J. Phys. Chem. A 105 (2001) 7865.
[19] R. Volkamer, P. Spietz, J. Burrows, U. Platt, J. Photochem. Photobiol. A 172 (2005) 35.
[20] R. Volkamer, L.T. Molina, M.J. Molina, T. Shirley, W.H. Brune, Geophys. Res. Lett. 32 (2005) L08806, doi:10.1029/2005GL022616.
[21] S. Beirle, R. Volkamer, F. Wittrock, A. Richter, J. Burrows, U. Platt, T. Wagner, DOAS Retrieval of Glyoxal from Space, Proceeding at ESA Workshop, 2006, http://earth.esrin.esa.it/workshops/atmos2006/ participants/1055/paper_DOAS_retrieval_of_Glyoxal_from_space.pdf.
[22] F. Wittrock, A. Richter, H. Oetjen, J.P. Burrows, M. Kanakidou, S. Myriokefalitakis, R. Volkamer, S. Beirle, U. Platt, T. Wagner, Geophys. Res. Lett. 33 (2006) L16804, doi:10.1029/2006GL026310.
[23] H.J. Jost, K. Drdla, A. Stohl, L. Pfister, M. Loewenstein, J.P. Lopez, P.K. Hudson, D.M. Murphy, D.J. Mahoney, D.J. Cziczo, M. Fromm, T.P. Bui,

J. Dean-DAY, C. Gerbig, M.J. Mahoney, erik C. Richard, N. Spichtinger, J.V. Pittman, E.M. Weinstock, J.C. Wilson, I. Xueref, Geophys. Res. Lett. 31 (2004) L11101, doi:10.1029/2003GL019253.
[24] G. Luderer, J. Trentmann, T. Winterrath, C. Textor, M. Herzog, H.F. Graf, M.O. Andreae, Atmos. Chem. Phys. 6 (2006) 5247.
[25] I. Pison, L. Menut, Atmos. Environ. 38 (2004) 971.
[26] C. Guimbaud, D. Labonnette, V. Catoire, R. Thomas, Int. J. Mass Spectrom. 178 (1998) 161.
[27] V. Catoire, E. Michel, C. Guimbaud, D. Labonnette, G. Poulet, Int. J. Mass Spectrom. Ion Process 243 (2005) 141.
[28] D.A. Fairley, D.B. Milligan, C.G. Freeman, M.J. McEwan, P. Španěl, D. Smith, Int. J. Mass Spectrom. 193 (1999) 35.
[29] D. Smith, A. Diskin, P. Španěl, Int. J. Mass Spectrom. 209 (2001) 81.
[30] P. Španěl, D. Smith, J. Am. Soc. Mass Spectrom. 12 (2001) 863.
[31] N. Schoon, C. Amelynck, L. Vereecken, E. Arijs, Int. J. Mass Spectrom. 229 (2003) 231.
[32] N. Schoon, C. Amelynck, L. Vereecken, H. Coeckelberghs, E. Arijs, Int. J. Mass Spectrom. 239 (2004) 7.
[33] L.M. Dobeck, H.M. Lambert, W. Kong, P.J. Pisano, P.L. Houston, J. Phys. Chem. A 103 (1999) 10312.
[34] G.K. Moortgat, W. Seiler, P. Warneck, J. Chem. Phys. 78 (1983) 1185.
[35] W. Forst, Quantum Chem. Program. Exch. 13 (1993) 21 (Program FALLOFF, 1993, QCMP 119).
[36] W. Forst, Unimolecular Reactions: A Concise Introduction, Cambridge University Press, Cambridge, UK, 2003.
[37] R.G. Gilbert, S.C. Smith, Theory of Unimolecular and Recombination Reactions, Blackwell Scientific Publications, Oxford, UK, 1990.
[38] M.J. Frisch, G.W. Trucks, H.B. Schlegel, G.E. Scuseria, M.A. Robb, J.R. Cheeseman, V.G. Zakrzewski, J.A. Montgomery Jr., R.E. Stratmann, J.C. Burant, S. Dapprich, J.M. Millam, A.D. Daniels, K.N. Kudin, M.C. Strain, O. Farkas, J. Tomasi, V. Barone, M. Cossi, R. Cammi, B. Mennucci, C. Pomelli, C. Adamo, S. Clifford, J. Ochterski, G.A. Petersson, P.Y. Ayala, Q. Cui, K. Morokuma, D.K. Malick, A.D. Rabuck, K. Raghavachari, J.B. Foresman, J. Cioslowski, J.V. Ortiz, A.G. Baboul, B.B. Stefanov, G. Liu, A. Liashenko, P. Piskorz, I. Komaromi, R. Gomperts, R.L. Martin, D.J. Fox, T. Keith, M.A. Al-Laham, C.Y. Peng, A. Nanayakkara, C. Gonzalez, M. Challacombe, P.M.W. Gill, B. Johnson, W. Chen, M.W. Wong, J.L. Andres, C. Gonzalez, M. Head-Gordon, E.S. Replogle, J.A. Pople, Gaussian 98, Revision A.7 ed., Gaussian, Inc., Pittsburgh, PA, 1998.
[39] A.D. Becke, J. Chem. Phys. 98 (1993) 5648.
[40] C. Lee, W. Yang, R.G. Parr, Phys. Rev. B 37 (1988) 785.
[41] National Institute of Standards and Technology, in: R.D. Johnson III (Ed.), Computational Chemistry Comparison and Benchmark DataBase, NIST Standard Reference Database 101, Release 12, August 2005 (http://srdata.nist.gov/cccbdb/).
[42] T. Su, W.J. Chesnavitch, J. Chem. Phys. 76 (1982) 5183.
[43] T. Su, J. Chem. Phys. 88 (1988) 4102.
[44] M. Henchman, in: P. Ausloos, S.G. Lias (Eds.), Entropy-driven Reactions: Summary of the Panel Discussion in Structure/Reactivity and Thermochemistry of Ions, NATO ASI Series, Series C: Mathematical and Physical Sciences, vol. 193, D. Reidel Publishing Company, Dordrecht, Holland, 1987.
[45] E.L. Coitino, J. Tomasi, Chem. Phys. 204 (1996) 391.
[46] D. Smith, T. Wang, P. Španěl, Rapid Commun. Mass Spectrom. 17 (2003) 2655.
[47] A.G. Harrison, Chemical Ionisation Mass Spectrometry, second ed., CRC Press, Boca Raton (FL), USA, 1992.
[48] K.A. Holbrook, M.J. Pilling, S.H. Roberston, Unimolecular Reaction, second ed., John Wiley & Sons Ltd., Chichester, 1996.
[49] E. Ruiz, D.R. Salahub, A. Vela, J. Phys. Chem. 100 (1996) 12265.
[50] P. Španěl, J.M. Van Doren, D. Smith, Int. J. Mass Spectrom. 213 (2002) 163.
[51] J. Troe, J. Phys. Chem. 114 (1979).
[52] W.C. Gardiner, J. Troe, in: W.C. Gardiner (Ed.), Combustion Chemistry, Springer Verlag, Berlin, 1984.
[53] A.F. Wagner, D.M. Wardlaw, J. Phys. Chem. 92 (1988) 2462.
[54] Y. Ikezoe, S. Matsuoka, M. Takebe, A. Viggiano, Gas Phase Ion-Molecule Reaction Rate Constants Through 1986, Maruzen Company Ltd., Tokyo, 1987.
[55] V. Marécal, G. Durry, K. Longo, S. Freitas, E. Rivière, M. Pirre, Atmos. Chem. Phys. Discuss. 6 (2006) 8241.
[56] L. Jaeglé, D.J. Jacob, W.H. Brune, I. Faloona, D. Tan, B.G. Heikes, Y. Kondo, G.W. Sachse, B. Anderson, G.L. Gregory, H.B. Singh, R. Pueschel, G. Ferry, D.R. Blake, R. Shetter, J. Geophys. Res. A 105 (2000) 3877.
[57] T.J. Christian, B. Kleiss, R.J. Yokelson, R. Holzinger, P.J. Crutzen, W.M. Hao, T. Shirai, D.R. Blake, J. Geophys. Res. A 109 (2004), doi:10.1029/2003JD00387.
[58] E. Arijs, A. Barassin, E. Kopp, C. Amelynck, V. Catoire, H.P. Fink, C. Guimbaud, U. Jenzer, D. Labonnette, W. Luithardt, E. Neefs, D. Nevejans, N. Schoon, A.M. Van Bavel, Int. J. Mass Spectrom. Ion Process 181 (1998) 99.
[59] D.R. Lide (Ed.), Handbook of Chemistry and Physics, 79th ed., CRC Press, Boca Raton, 1998.
[60] P. Španěl, D. Smith, Int. J. Mass Spectrom. 181 (1998) 1.
[61] P.F. Wilson, C.G. Freeman, M.J. McEwan, Int. J. Mass Spectrom. 229 (2003) 143.
[62] P. Španěl, D. Smith, J. Chem. Phys. 104 (1996) 1893.
[63] S.T. Arnold, A.A. Viggiano, R.A. Morris, J. Phys. Chem. A 102 (1998) 8881.